PCCP

Accepted Manuscript




ROYAL SOCIETY OF CHEMISTRY

www.rsc.org/pccp

# Mechanism of Excited-State Proton Transfer in 1-Naphthol‑Piperidine Clusters

Toshihiko Shimizu,[a] Shun Manita,[a] Shunpei Yoshikawa,[a] Kenro Hashimoto,[b] Mitsuhiko Miyazaki[a] and Masaaki Fujii*[a]

[a] Chemical Resources Laboratory, Tokyo Institute of Technology, 4259 Nagatsuta, Midori-ku, Yokohama 226-8503, Japan,

[b] Department of Chemistry, Graduate School of Science and Engineering, Tokyo Metropolitan University, 1-1 Minami-Osawa, Hachioji, 192-0397, Japan

*: Corresponding Author, e-mail: mfujii@res.titech.ac.jp.

**Abstract**

The geometries of 1-naphthol–(piperidine)$_n$ (1-NpOH–(Pip)$_n$) ($n$ = 0-3) clusters have been calculated by using density functional theory (DFT) and time-dependent density functional theory (TD-DFT) methods to investigate excited-state proton transfer (ESPT) in the low-lying singlet excited states, $L_a$ and $L_b$. For the $n$ = 1 cluster, no PT structure was found in $L_b$ and $L_a$ as well as the ground state, $S_0$. For $n$ = 2, optically accessible $L_b$ from $S_0$ shows the PT structure. We therefore concluded that the threshold size of ESPT is $n$ = 2, which is consistent with previous experimental results. ESPT in 1-NpOH–(Pip)$_n$ is simply triggered by optical excitation to $L_b$. It is essentially different from the 1-NpOH–(NH$_3$)$_n$ cluster in which an internal conversion process is required to promote ESPT. From the calculated structures, the importance of the solvation of the π-ring is strongly suggested rather than the proton affinity in ESPT.

**Keywords:**

cluster; proton transfer; excited state calculations; naphthol; piperidine

## 1. Introduction

The proton transfer reaction along the hydrogen-bond is one of the most important reactions in chemistry and biology. Particularly the excited-state proton transfer (ESPT) reaction attracts many researchers[1-5] because it can be controllable by photoexcitation. For phenol, ESPT was expected both in solution and solvated clusters; however, it was found that the H atom was moved to the solvent moiety (ESHT) instead of the proton, at least in solvated clusters.[6-18] For naphthol (NpOH), ESPT was found in aqueous solution by visible emission after UV excitation,[19, 20] and its solvent effect and relation to the level crossing dynamics were extensively studied by an ultrafast spectroscopy. The origin of the visible emission was interpreted as being the formation of an anion such as $NpO^-$; thus, this emission was interpreted as involving the release of a proton in the excited state. Such a proton release corresponds to an increase of the acidity, and thus the p$K_a$ values of 1-NpOH were assumed to decrease by $S_1 \leftarrow S_0$ excitation, such as 9.1 ($S_0$) to 0.5 ($S_1$) in 1-NpOH. Considering the drastic decrease of p$K_a$ by photoexcitation, naphthols and related molecules including phenols are called photoacids. However, further detailed mechanics of ESPT, such as the effect of the orientation and the relation to the electronic states, has not been revealed in any spectroscopic study in solution.

A molecular cluster generated in a supersonic jet enables us to study chemical reactions with well-defined initial states. The number of molecules in a cluster can be specified and their orientations are fixed in the cluster. Various laser spectroscopies have been applied solvated clusters in order to elucidate the mechanism of ESPT at the molecular level. For example, ESPT and related phenomena have been examined for phenol–$(H_2O)_n$/$(NH_3)_n$, 1-NpOH–$(H_2O)_n$/$(NH_3)_n$/(piperidine)$_n$, 2-NpOH–$(H_2O)_n$/$(NH_3)_n$, hydroxyquinoline–$(NH_3)_n$, 7-azaindole–$(NH_3)_n$ and other systems by laser-induced fluorescence (LIF), dispersed fluorescence, resonant enhanced multiphoton ionization (REMPI), ion dip IR spectroscopy, time-resolved pump-probe experiments, picosecond time-resolved IR dip spectroscopy, and so forth.[21-46] It has been found that ESPT takes place in small 1-NpOH clusters with strong bases (ammonia and piperidine).[47-49]

ESPT in 1-naphthol–(piperidine)$_n$ (1-NpOH–(Pip)$_n$) has been investigated by using the same strategy as that for 1-NpOH–$(NH_3)_n$ clusters. These 1-NpOH–(Pip)$_n$ clusters are important because they require only fewer solvent molecules than 1-NpOH–$(NH_3)_n$ clusters to promote ESPT, due to its higher basicity. Thus, they have been considered to be one of the prototype systems for ESPT. The first evidence of ESPT in 1-NpOH–(Pip)$_n$ clusters was found in dispersed fluorescence spectra.[47] The $n$ = 2 cluster shows a broad, strongly red-shifted spectrum, which is close to the spectrum of $NpO^-$ in a basic solution.[47] Cheshnovsky and Leutwyler concluded that the minimum size necessary to promote ESPT is $n$ = 2 for 1-NpOH–(Pip)$_n$. Zewail's group also concluded that the minimum size is $n$ = 2 based on the cluster size dependence on the lifetime.[26]

Through various experimental studies, the ESPT mechanism in 1-NpOH clusters has often been discussed in terms of the two-step three-state model. The naphthalene ring has $L_a$ and $L_b$ electronic states, and $L_b$ is the lowest excited state in the monomer.[50] The polar $L_a$ state is stabilized by solvation and the energy order can be reversed. If the cluster is excited to the $L_b$ state by an optical transition, the internal conversion to $L_a$ (1st step) triggers proton transfer (2nd step). Recent progress of computer technology and time-dependent density functional theory (TD-DFT) enable us to study structures, vibrations and chemical reactions in excited molecules at a sufficient level. We have studied the ESPT mechanism of 1-NpOH–$(NH_3)_n$ by applying TD-DFT at the M06-2X/cc-pVDZ level in the $L_b$ and $L_a$ states. The cluster size dependence of ESPT was investigated based on vertical transitions from the geometries that can be populated in molecular-beam experiments. For the $n$ = 3 and 4 clusters, the proton-transferred geometries cannot be accessible without a significant geometrical rearrangement from the initially populated isomers. For the $n$ = 5 clusters, the proton-transferred structure is found in the $L_a$ excited state of the isomer that can be populated in the beam. Thus, ESPT is possible by an optically prepared $L_b$ state via internal conversion to $L_a$. Therefore, the two-step three-state model is confirmed, and the threshold cluster size of ESPT is concluded to be $n$ = 5 under the experimental condition of low excess energy.

To establish the ESPT mechanism, another benchmark system of ESPT has to be studied based on theoretical calculations. Here, we applied the TD-DFT methods to 1-NpOH–$(Pip)_n$, and revealed the ESPT mechanism in terms of the structures and electronic states with restriction of the optical transitions. Surprisingly, our theoretical analysis shows that 1-NpOH–$(Pip)_n$ does not follow the two-step three-state model, and thus a simpler mechanism is concluded. A structural analysis suggests that solvation of the π-ring is important in ESPT.

## 2. Methods

Molecular structures of 1-NpOH–$(Pip)_n$ ($n$ = 0-3) in $S_0$ were optimized by using the DFT method. The M06-2X/cc-pVTZ level of approximation was used in the geometry optimization. The initial geometries were generated based on the smaller cluster by adding a piperidine molecule to the possible hydrogen-bonding sites. Since these clusters are relatively small, we can pick up possible hydrogen-bonded structures. Geometry optimizations of $L_b$ and $L_a$ were carried out at the TD-M06-2X/cc-pVDZ level. Single point energy calculations were performed on the optimized geometries with CISD/LanL2DZ. The equilibrium configurations that are stable in $S_0$ were used as initial configurations to optimize the structures in $L_b$ and $L_a$. Here, $L_b$ and $L_a$ were distinguished by the direction of the dipole moment[50] and the shapes of relevant molecular orbitals (MO). The convergence to the energy minimum was checked by calculating the vibrational frequencies. All of the structures have been confirmed to have all real vibrational frequencies. The relative solvation

enthalpies at 0 K were computed with the zero-point vibrational correction by the scaling factors 0.943 and 0.948 for the ground and excited states, respectively. These values were determined from the $\nu_{OH}$ ratio of the experimental and computational frequencies of the 1-NpOH monomer. The basis set superposition error (BSSE) was assessed by the counterpoise (CP) method. The program used was Gaussian 09.[51]

## 3. Results and Discussion

### A. Structures of 1-NpOH–(Pip)$_n$ ($n$ = 0−3) in the ground and excited states.

The optimized geometries and their relative energies of 1-NpOH–(Pip)$_n$ ($n$ = 0 and 1) in $S_0$, $L_b$, and $L_a$ are shown in Fig. 1. The optimized geometry **Oa** of *trans*-1-NpOH has $C_s$ symmetry; an OH bond length is 0.961 Å; however, the optimized geometry **Ob** of *cis*-1-NpOH has $C_1$ symmetry, and the OH bond length is 0.959 Å. The *cis*-1-NpOH is less stable by 1.2 kcal/mol relative to *trans*-1-NpOH in $S_0$, whereas the *cis*-1-NpOH is more stable than *trans*-1-NpOH in both the $L_b$ and $L_a$ ππ* states. This inversion of the relative energies is consistent with experimental estimations.[52]

For the $n$ = 1 clusters, we have found three isomers in the ground state: **Ia**, **Ib**, and **Ic**. In the structure of **Ia,** *trans*-1-NpOH acts as a proton donor. The OH bond length is 0.993 Å in $S_0$, while it is elongated to 1.012 and 1.023 Å in $L_b$ and $L_a$, respectively. These bond lengths are longer than that of 1-NpOH–$(NH_3)_1$ (0.982, 0.996 and 1.002 Å for $S_0$, $L_b$ and $L_a$, respectively). The longer bond length than that in 1-NpOH–$(NH_3)_1$ is consistent to the higher proton affinity of piperidine.[48] The second isomer **Ib**, *cis*-1-NpOH–$(Pip)_1$, is 0.7 kcal/mol more unstable than the *trans*-1-NpOH–$(Pip)_1$ (**Ia**). The last isomer **Ic**, in which *trans*-1-NpOH acts as a proton-acceptor, is 7.6 kcal/mol more unstable than **Ia**. For the $n$ = 1 clusters, **Ia** and **Ib** may coexist in a supersonic jet because of small differences of the relative energies.

For $n$ = 2, six isomers, **IIa**–**IIf**, in $S_0$ are identified as shown in the left column of Fig. 2. Complexes **IIa** and **IId** are chain structures in which a piperidine dimer is bound to 1-NpOH by a OH-N H-bond. Here, the 1-NpOH molecule is the *cis*-form in **IIa** and the *trans*-form in **IId**, both of which act as a proton donor. The second piperidine molecule locates close to the aromatic ring. This suggests stabilization by the NH-π interaction in **IIa** and **IId**. In the structures **IIb**, **IIc**, and **IIe**, the complexes have cyclic structures based on a H-bond network: O⁻H→N–H→N–H→O. The 1-NpOH molecule is the *trans*-form in **IIb** and **IIc**, while it is the *cis*-form in **IIe**. In the structure **IIf**, 1-NpOH acts not only as a proton donor, but also as a proton acceptor, where no interaction is found between two piperidine molecules. **IIa** is the most stable, and the relative energies to **IIb**–**IIf** are 1.7, 2.78, 2.83, 3.5 and 6.2 kcal/mol, respectively. The population will thereby be concentrated to structure **IIa** in a molecular beam.

In the $L_b$ excited state, **IIa$_{Lb}$** holds the chain structure, however the proton in NpOH is transferred to the piperidine moiety (PT-type). It is the most stable structure as well as in $S_0$, and the energy difference becomes larger. The second stable structure is **IIb$_{Lb}$** but its unstability is enhanced from 1.7 kcal/mol in $S_0$ to 3.2 kcal/mol in $L_b$. Similarly, in the $L_a$ state, **IIa$_{La}$** has the PT-type structure, which is the most stable one. The relative energy differences to other structures are enhanced by three times. The second stable **IIb$_{La}$** is now 9.7 kcal/mol more unstable than **IIa$_{La}$**. In the $L_b$ state, the naphtholic proton in the most stable structure, **IIa$_{Lb}$**, locates 1.522 Å from the oxygen atom, and forms piperidine-$H^+$. In the other structures, since the proton in naphtholic OH is still close to the 1-NpOH molecule, no ESPT is found. On the other hand, the naphtholic proton in the most stable structure in the $L_a$ state (**IIa$_{La}$**) locates at 1.663 Å from the oxygen atom, and also forms piperidine-$H^+$, while no ESPT is found in other isomers as well as in the $L_b$ state. Accordingly, $n$ =2 can be the smallest cluster for the ESPT reaction. The non-ESPT structures, **IIb$_{La}$**–**IIf$_{La}$**, are more unstable than the ESPT one; thus, the proton transfer significantly contributes to stabilization of the clusters in $L_a$.

The left column of Fig. 3 displays eight equilibrium structures, **IIIa**–**IIIh**, for the $n$ = 3 clusters in $S_0$. All of them are the *trans*-form except structure **IIIc**, which is the *cis*-form. Complexes **IIIa** and **IIIb** have a cyclic H-bond network. Structure **IIIa** is more stable than **IIIb** by 1.9 kcal/mol. **IIIc** is a structure in which the third piperidine molecule is bound to the **IIa** structure from the opposite side of the two-membered piperidine moiety to the O atom in 1-NpOH. It is 4.0 kcal/mol less stable than **IIIa**. In **IIId**, piperidine molecules locate at both sides of 1-NpOH, likely to **IIIc**, but 1-NpOH has the trans-form. It is less stable than **IIIa** by 4.6 kcal/mol. In **IIIc**, the NH bond in piperidine interacts with an aromatic ring of 1-NpOH, while the CH bond locates toward the π-ring in **IIId**. Complex **IIIe** is a bifurcated structure where a three-membered piperidine chain is bound to 1-NpOH through a single H-bond of the central piperidine molecule. The energy for **IIIe** is 8.5 kcal/mol less stable relative to **IIIa**. Regarding structure **IIIf**, 1-NpOH acts as a proton donor for the first piperidine, and piperidine dimer is bound to the first piperidine by a van der Waals interaction. The energy for **IIIf** is higher than that of **IIIa** by 9.81 kcal/mol. The other two isomers, **IIIg** and **IIIh**, have chain H-bond structures in piperidine moieties, but CH bonds also participate in the network of these isomers. The energies of both isomers are 9.84 kcal/mol higher than that of **IIIa**.

The optimized structures for the $n$ = 3 clusters in $L_b$ and $L_a$ are also depicted in the center and the right columns of Fig. 3. As can be seen in the figure, all of the complexes have a H-bond network similar to those in $S_0$, regardless of the electronic states. The relative energies to **IIIa$_{Lb}$** of the complexes in the $L_b$ state are indicated in the figure. For the $L_a$ state, the most stable isomer is **IIId$_{La}$**, and thus the energies are the relative energies to that of **IIId$_{La}$**. The most significant

difference from the structures in $S_0$ is the location of the H atom in the naphtholic OH. In the $L_b$ state, the naphtholic proton in the most stable structure **IIIa$_{Lb}$** locates 1.493 Å from the oxygen atom, and forms piperidine-$H^+$. Such an ESPT is also found in the structure **IIIc$_{Lb}$**. The naphtholic proton in the most stable structure in the $L_a$ state (**IIId$_{La}$**) locates 1.830 Å from the oxygen atom, and also forms piperidine-$H^+$. ESPT are also found in structures **IIIa$_{La}$** and **IIIc$_{La}$**. The non-ESPT structures, **IIIb$_{La}$** and **IIIe$_{La}$**–**IIIh$_{La}$**, are more unstable than the ESPT ones, and thus the proton transfer stabilizes the clusters in $L_a$.

**B. Mechanism of ESPT**

We have elucidated the energy relationship in each of the $S_0$-, $L_b$- and $L_a$-optimized geometries for 1-NpOH–$(Pip)_n$ ($n$ = 0-3). In this section, we consider the ESPT mechanism and the relation to the observed photochemical reactivity. It is necessary to calculate the vertical transition energies from $S_0$ to the electronic excited states when we will discuss the observed size dependence of ESPT. Here, we calculated the vertical transition energies to the $L_b$ and $L_a$ states at the optimized structures in the $S_0$ state. The vertical transition energies were calculated at CISD/LanL2DZ level. To compare the energies between the vertical and optimized geometries in $L_b$, it is necessary to calculate the energies of $S_0$ and $L_a$ at the $L_b$-optimized ($L_b$-opt) structure. Similarly the energies of $S_0$ and $L_b$ were calculated for the $L_a$-optimized structure. If we add the energies of $S_0$ to those of $L_a$ and $L_b$, it is possible to compare the $L_b$ and $L_a$ energies among isomers. Then, all of the calculated energies are presented based on the energy of $S_0$ in the most stable isomers (**Ia, IIa** and **IIIa**) for $n$ = 1-3, respectively.

All of the calculated results for $n$ = 1 are represented in Fig. 4(a). Concerning the most stable species, **Ia**, the vertical transition energies, $L_b$ and $L_a$, are shown in the left column with the color of purple and red horizontal bars; this set of energies is indicated as $S_0$-opt. The energies $L_a$ and $L_b$ at the optimized structure for the $L_b$ state are plotted in the center column ($L_b$-opt) after an energy correction to $S_0$. Similarly, the energies of $L_a$ and $L_b$ at the $L_a$-optimized structure were shown in the right column ($L_a$-opt). The same set of energies ($S_0$-, $L_b$- and $L_a$-opt) is also shown for each isomer.

In the $S_0$ state, the population is thought to distribute to **Ia** and **Ib**, because the second stable species, **Ib**, is only 0.7 kcal/mol unstable from **Ia**. It was not discussed in previous experimental reports;[48, 53] however, the reported REMPI spectrum presents complicated vibronic structures, and thus the coexistence of two species would not be surprising. We thus consider the excitation of both **Ia** and **Ib**. The vertical transitions from **Ia** and **Ib** prepare the non-PT $L_b$ states. The optimized structures of $L_b$ are more stable than that of $L_a$ in both isomers. Therefore, the excited cluster will stay in $L_b$, and no PT will be expected in this geometry. Regarding **Ic** isomers, proton-transferred

structures were not found in any state, and thus no ESPT is expected for $n$ = 1. This is consistent with the experimental results.

Fig. 4(b) shows the energies of the $S_0$, $L_b$ and $L_a$ states in the $n$ = 2 clusters. The clusters will be populated in **IIa** for $S_0$, because the second stable species, **IIb**, is 1.7 kcal/mol more unstable than **IIa**. The vertical transition from **IIa** in $S_0$ will prepare the $L_b$ state. Because the $L_b$ state has the PT structure, the optical transition immediately induces PT. The $L_a$ state is slightly more unstable than $L_b$ in $L_b$-opt; however, it is significantly stabilized when the geometries are optimized for the $L_a$ state. Thus, the photoexcitation of **IIa** finally produces the $L_a$ state, which has also the PT geometry. This is consistent with the experimentally proposed size-dependence $n$=2. It should be noted that the PT structures are found only in the **IIa** isomer.

Similarly to the $n$ = 2 clusters, the ground state population is limited to the most stable isomer, **IIIa**, in the $n$ = 3 clusters, because the second most stable species is 1.9 kcal/mol unstable (see Fig. 4(c)). The PT structures are found in both the $L_b$ and $L_a$ states of isomers **IIIa** and **IIIc** and in the $L_a$ state of isomer **IIId**. The vertical excitation of **IIIa** will produce the $L_b$ state, which has the PT geometry. This means that the photoexcitation directly triggers PT. The energy of the $L_a$ state is more stable than $L_b$ in the $L_a$-optimized geometries, and thus finally the photoexcited **IIIa** cluster will be in the $L_a$ state, which has the PT structure. Although no experimental result has been reported, the calculated results predict ESPT in the $n$ = 3 clusters as well as $n$ = 2.

We have found from theoretical calculations that the threshold size of ESPT for 1-NpOH–$(Pip)_n$ is $n$ = 2, regardless of the excess energy in $S_1$, whereas the threshold size of 1-NpOH–$(NH_3)_n$ is $n$ = 5 under the low excess energy conditions. The ESPT mechanism in 1-NpOH–$(NH_3)_n$ clusters has been explained by the two-step three-state model.[54] 1-NpOH has the $L_a$ and $L_b$ electronic states and $L_b$ is the lowest excited state in the monomer. In the $n$ = 5 clusters, the $L_b$ state, which can be prepared by the optical transition from $S_0$, has the non-PT structure, while the $L_a$ state has the PT structure. The polar $L_a$ state is stabilized more than that of $L_b$ by solvation, and the energy order is reversed. Thus internal conversion from $L_b$ to $L_a$ (1st step) triggers proton transfer (2nd step). On the contrary, for 1-NpOH–$(Pip)_n$ clusters, the $L_b$ state, itself, has the PT structure. Therefore, the electronic relaxation, i.e., the internal conversion, process is not needed in this case. We calculated the potential-energy curves in the $S_0$, $L_b$ and $L_a$ states of the IIa isomer along the OH distance, and found that no barrier exist between the Franck-Condon region and the most stable PT structure in the excited states (see Fig. S1 in Supplementary Information). This fact demonstrates that the ESPT mechanism in 1-NpOH–piperidine clusters is essentially different from that in 1-NpOH–ammonia clusters. It should be noted that the effects of long-range solvent interactions must be taken into account when we extend the results to ESPT in a solution.[55]

Let us discuss the relation between the structures of the clusters and the proton transfer. 1-NpOH has two major binding motifs: the hydrogen-bond of the OH group and the dispersion / π hydrogen-bond from the aromatic ring. The structures of the clusters are determined by their balance. We focus on typical isomers of the PT structure (**IIa**) and the non-PT structure (**IIb**) in Fig. 2. In the non-PT isomer (**IIb**), the solvent molecules are bound at the OH group, and form a cyclic hydrogen-bond network. This structure is mainly governed by the hydrogen-bond, and the interaction from the aromatic ring does not contribute very much. On the other hand, in the PT structure (**IIa**), the solvent molecules locate on the naphthalene ring. This structure suggests that both the hydrogen-bonding of the OH group and the dispersion / π hydrogen-bond from the aromatic ring stabilize isomer **IIa**. In the 0th-order approximation, the hydrogen-bond to the OH group forms a local network, which will not affect the electronic state very much. The interaction to the aromatic ring through the dispersion / π hydrogen bond would cause direct perturbations to the ππ* electronic excited states. In this sense, the solvation of the naphthalene ring is important on the PT reaction, rather than the local solvation of the OH group.

The interaction between the aromatic ring and the solvent molecules can be estimated based on the distance between them. The shortest distance, from the carbon atoms of the naphthalene ring to the hydrogen atoms of solvents, were measured in all of the calculated isomers in $S_0$, $L_b$ and $L_a$. These are summarized in Table 1. Here, numbers in italic means that the isomer has the PT structure, and the capital letter C or N represents the shortest distance is given by N–H or C–H bonds, respectively. As can be seen in the table, all of the PT isomers have shorter distances than that of the non-PT structures. Thus, the shortest distance can be a good parameter for the PT reaction. The threshold value of the PT reaction is 2.51 Å for the 1-NpOH–$(Pip)_n$ clusters. It is interesting that all of the PT structures show the shortest distance by N–H bonds.

The same analysis has been applied to the 1-NpOH–$(NH_3)_n$ clusters, of which the structures were calculated in previous work.[56] Table 2 summarizes the shortest distances in the isomers of the 1-NpOH–$(NH_3)_n$ ($n$ = 3-5) clusters in $S_0$, $L_b$ and $L_a$. Again, the PT structures show smaller values of the shortest distance than those in the non-PT isomers. The threshold value, 2.52 Å, is very close to that in 1-NpOH–$(Pip)_n$. Such consistent results strongly suggest that the shortest distance between the aromatic system and the solvent molecules can be a general indicator for the PT reaction. From these analyses, we would like to emphasize that solvation of the aromatic ring is essential for the PT reaction for hydroxyl aromatics systems.

## 4. Conclusions

We have discussed the size dependence of ESPT in 1-NpOH–$(Pip)_n$ clusters. We found 3, 6 and 8 stable isomers for the clusters of $n$ = 1, 2 and 3. From the calculated relative energies in $S_0$,

the initial population was estimated. For $n$ = 1, the population is distributed to isomers **Ia** and **Ib**. For $n$ = 2 and 3, the population is concentrated to the most stable isomer, **IIa** and **IIIa**, respectively. Optical transitions from these initial isomers always produce the $L_b$ states. For the $n$ = 1 clusters, the optimized structure of $L_b$ is more stable than that of $L_a$ in **Ia** and **Ib**. Thus, the excited cluster will stay in $L_b$, and no ESPT will be expected in $n$ = 1.

In the case of 1-NpOH–$(Pip)_2$, the PT structure is found in both the $L_b$ and $L_a$ states of the initially populated isomer **IIa**. Thus, the vertical excitation of **IIa** will produce the $L_b$ state, which has the PT geometry. This means that the photoexcitation directly triggers PT. The energy of the $L_a$ state is more stable than $L_b$ in the $L_a$-optimized geometry. Thus, finally the photoexcited **IIa** cluster will be in the $L_a$ state, which also has the PT structure. This situation is completely different from the case in 1-NpOH–$(NH_3)_n$ clusters, in which the PT mechanism is explained by the two-step three-state model, where PT is triggered by the internal conversion from $L_b$ to $L_a$. The ESPT mechanism in $n$ = 3 is the same as that in $n$ = 2. Therefore, we concluded that the threshold size of ESPT is $n$ = 2 in 1-NpOH–$(Pip)_n$. These theoretical conclusions are consistent with the experimental results.

It is also found that the shortest distance between the naphthalene ring and the solvents is a good indicator of the ESPT reaction. The threshold values of the PT reaction are 2.51 and 2.52 Å for the 1-NpOH–$(Pip)_n$ and 1-NpOH–$(NH_3)_n$ clusters, respectively. Usually the PT activity has been discussed in terms of the proton affinity of the solvent moiety. The proton affinity of ammonia is 208 kcal/mol, while that of piperidine is 228 kcal/mol. Thus, the smaller threshold size of 1-NpOH–$(Pip)_n$ appears to be consistent with the general understanding based on proton affinity. However, our calculations reveal that PT strongly depends on the structure of the cluster, and even in clusters having the same number of solvents, the ESPT does not take place in all clusters. This suggests that the solvation of the π-ring system is an essential key for the ESPT reaction, rather than the proton affinity.

**Acknowledgements**

This work was supported in part by KAKENHI on innovative area (2503) and the Cooperative Research Program of the "Network Joint Research Center for Materials and Devices" from the Ministry of Education, Culture, Sports, Science and Technology (MEXT), Japan, the Core-to-Core Program 22003 from the Japan Society for the Promotion of Science (JSPS). The computations were performed using Research Center for Computational Science, Okazaki, Japan.

**Figures and captions**

**Table 1** Caluculated values of the shortest distance from the naphthalene ring to the hydrogen atoms of solvents of 1-NpOH–$(Pip)_n$ in the $S_0$, $L_b$ and $L_a$ states. The numerical values of the PT-type isomers are in italic. The capital letter, C or N, represents the shortest distance is given by N–H or C–H bonds, respectively.

| isomer | $S_0$ | | $L_b$ | | $L_a$ | |
|---|---|---|---|---|---|---|
| 1a | 3.02 | C | 2.56 | C | 3.00 | C |
| 1b | 2.74 | C | 2.62 | C | 2.72 | C |
| 1c | 2.81 | C | 2.94 | C | 2.94 | C |
| 2a | 2.72 | N | *2.51* | N | *2.41* | N |
| 2b | 2.80 | C | 2.76 | C | 2.67 | N |
| 2c | 3.11 | C | 3.01 | C | 2.96 | C |
| 2d | 2.65 | N | 2.56 | N | 2.56 | N |
| 2e | 2.76 | C | 2.68 | C | 2.63 | C |
| 2f | 3.04 | C | 2.94 | C | 3.03 | C |
| 3a | 2.47 | C | *2.51* | N | *2.51* | N |
| 3b | 2.57 | N | 2.54 | N | 2.53 | N |
| 3c | 2.59 | N | *2.51* | N | *2.44* | N |
| 3d | 2.59 | N | 2.58 | N | *2.41* | N |
| 3e | 2.73 | C | 2.70 | C | 2.70 | C |
| 3f | 2.98 | C | 3.00 | C | 3.04 | C |
| 3g | 3.02 | C | 2.99 | C | 2.99 | C |
| 3h | 2.99 | C | 3.05 | C | 2.97 | C |

**Table 2** Caluculated values of the shortest distance from the naphthalene ring to the hydrogen atoms of solvents of 1-NpOH–$(NH_3)_n$ in the $S_0$, $L_b$, and $L_a$ states. The numerical values of the PT-type isomers are in italic.

| isomer | $S_0$ | $L_b$ | $L_a$ |
|---|---|---|---|
| 3a | 2.67 | 2.65 | 2.70 |
| 3b | 2.84 | 2.68 | *2.39* |
| 3c | 2.83 | 2.67 | 2.74 |
| 3d | 2.77 | 2.68 | *2.52* |
| 3e | 2.73 | 2.70 | *2.45* |
| 3f | 3.16 | 3.13 | 2.76 |
| 4a | 2.71 | 2.62 | 2.61 |
| 4b | 2.66 | 2.66 | 2.65 |
| 4c | 2.68 | 2.69 | *2.38* |
| 4d | 2.73 | 2.71 | 2.80 |
| 4e | 2.68 | 2.71 | 2.65 |
| 4f | 2.84 | *2.47* | *2.49* |
| 4g | 2.80 | 2.80 | *2.46* |
| 4h | *2.31* | *2.36* | *2.22* |
| 5a | 2.66 | 2.65 | *2.39* |
| 5b | 2.64 | 2.62 | *2.38* |
| 5c | 2.61 | 2.62 | *2.40* |
| 5d | 2.61 | *2.28* | *2.31* |
| 5e | 2.74 | *2.43* | *2.45* |
| 5f | 2.74 | 2.61 | *2.48* |
| 5g | *2.33* | *2.22* | *2.15* |

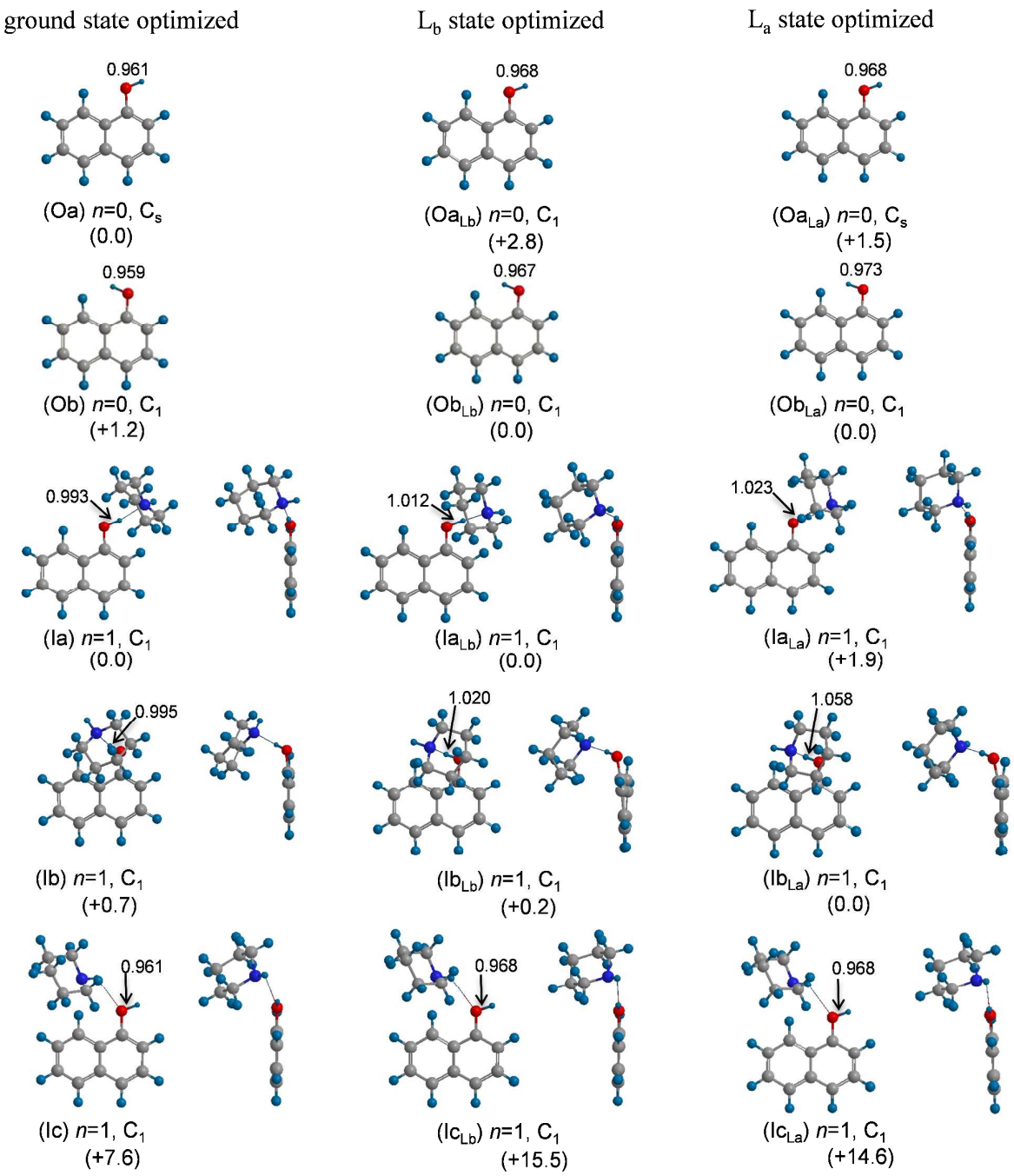


**Fig. 1** Calculated structures (left) of 1-NpOH–$(Pip)_n$ ($n$ = 0-1) in the ground state by DFT optimized at the M06-2X/cc-pVTZ level and those (center and right) in the $L_b$ and $L_a$ states by TD-DFT optimized at the M06-2X/cc-pVDZ level. Each length of the OH distance is given in angstroms. The relative energies are also presented in kcal/mol.

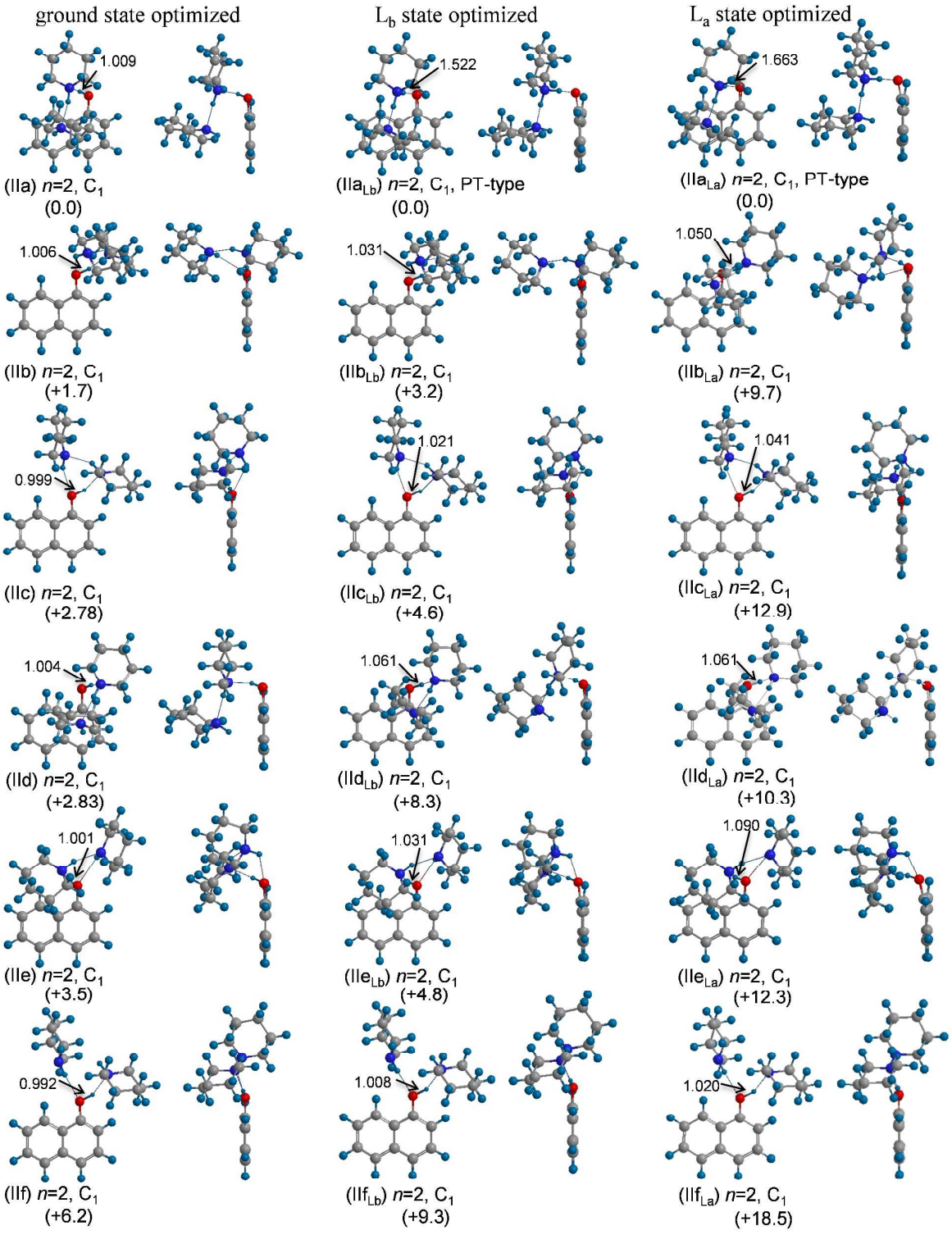


**Fig. 2** Calculated structures (left) of 1-NpOH–$(Pip)_2$ in the ground state by DFT optimized at the M06-2X/cc-pVTZ level and those (center and right) in the $L_b$ and $L_a$ states by TD-DFT optimized at the M06-2X/cc-pVDZ level. Each length of the OH distance is given in angstroms. The relative energies are also presented in kcal/mol.

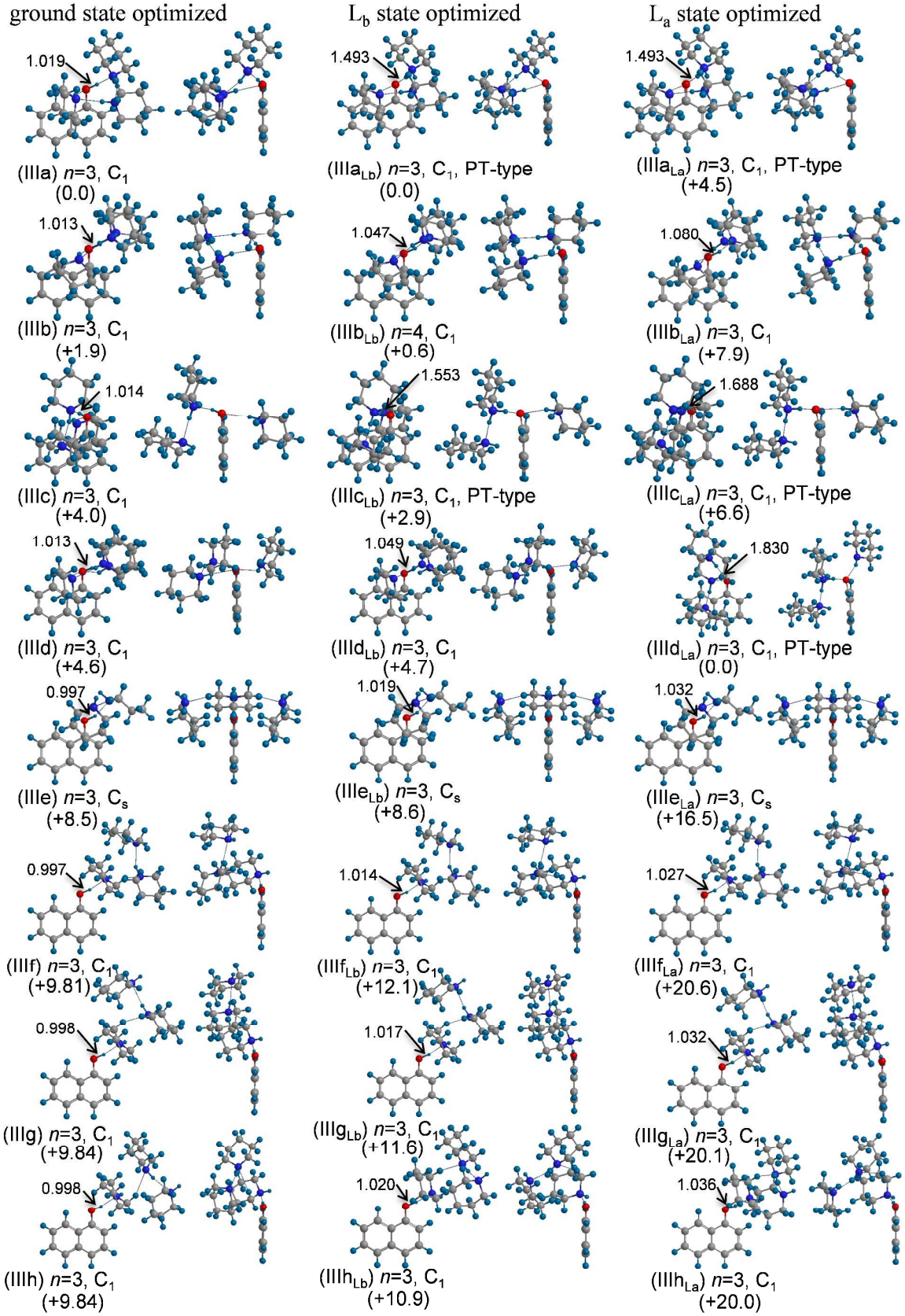


**Fig. 3** Calculated structures (left) of 1-NpOH–$(Pip)_3$ in the ground state by DFT optimized at the M06-2X/cc-pVTZ level and those (center and right) in the $L_b$ and $L_a$ states by TD-DFT optimized at the M06-2X/cc-pVDZ level. Each length of the OH distance is given in angstroms. The relative energies are also presented in kcal/mol.

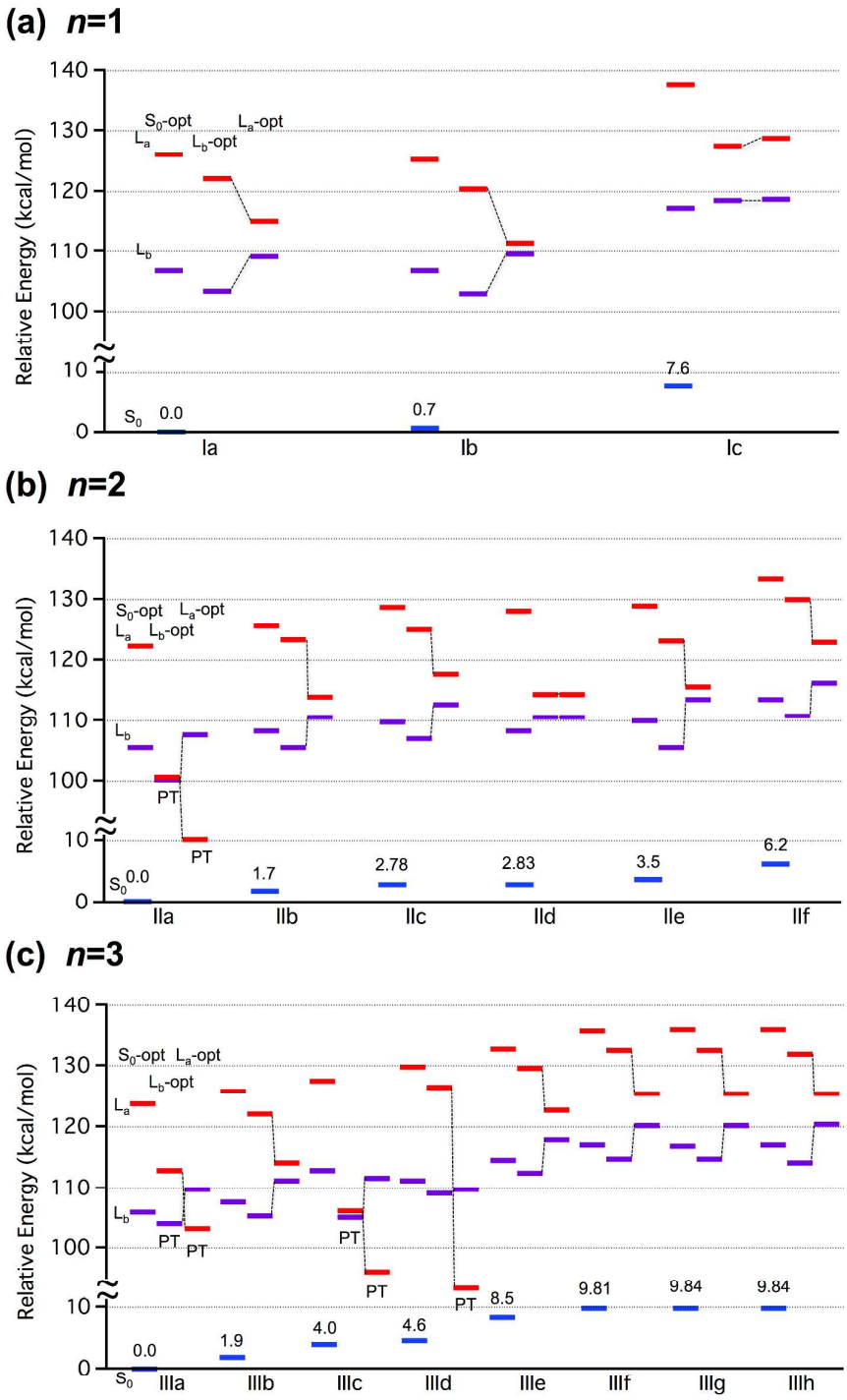


**Fig. 4** (a) Energetics diagram for the 1-NpOH–$(Pip)_1$ isomers relative to the energy of the ground state of the most stable $S_0$-optimized structure Ia, (b and c) corresponding to 1-NpOH–$(Pip)_2$ and 1-NpOH–$(Pip)_3$, respectively. The relative energies are plotted from the most stable species, IIa and IIIa, respectively. Calculated relative energies are presented in kcal/mol.

**Table of Contents Entry**

Photoexcitation directly triggers proton transfer in 1-naphthol–(piperidine)$_n$. This mechanism is essentially different from 1-naphthol–(NH$_3$)$_n$ in which the internal conversion process is required to promote excited-state proton transfer.

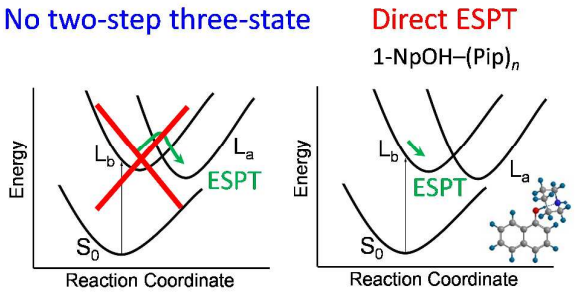

**References**


1. L. G. Arnaut and S. J. Formosinho, *J. Photochem. Photobiol. A: Chem.*, 1993, **75** 1-20.
2. L. M. Tolbert and K. M. Solntsev, *Acc. Chem. Res.*, 2002, **35**, 19-27.
3. J. de Klerk, A. Szemik-Hojniak, F. Ariese and C. Gooijer, *J. Phys. Chem. A*, 2007, **111**, 5828-5832.
4. B. Poór, N. Michniewicz, M. Kállay, W. J. Buma, M. Kubinyi, A. Szemik-Hojniak, I. Deperasińska, A. Puszko and H. Zhang, *J. Phys. Chem. A*, 2006, **110**, 7086-7091.
5. J. de Klerk, I. H. M. van Stokkum, A. Szemik-Hojniak, I. Deperasińska, C. Gooijer, H. Zhang, W.-J. Buma and F. Ariese, *J. Phys. Chem. A*, 2010, **114**, 4045–4050.
6. C. Dedonder-Lardeux, D. Grosswasser, C. Jouvet and S. Martrenchard, *Phys. Chem. Comm.*, 2001, **4**, 1-3.
7. C. Dedonder-Lardeux, D. Grosswasser, C. Jouvet, S. Martrenchard and A. Teahu, *Phys. Chem. Chem. Phys.*, 2001, **3**, 4316-4324.
8. S. Ishiuchi, K. Daigoku, M. Saeki, M. Sakai, K. Hashimoto and M. Fujii, *J. Chem. Phys.*, 2002, **117**, 7077-7082.
9. S. Ishiuchi, K. Daigoku, M. Saeki, M. Sakai, K. Hashimoto and M. Fujii, *J. Chem. Phys.*, 2002, **117**, 7083-7093.
10. S. Ishiuchi, M. Sakai, K. Daigoku, K. Hashimoto and M. Fujii, *J. Chem. Phys.*, 2007, **127**, 1-8.
11. K. Daigoku, S. Ishiuchi, M. Sakai, M. Fujii and K. Hashimoto, *J. Chem. Phys.*, 2003, **119**, 5149-5158.
12. W. Domcke and A. L. Sobolewski, *Science*, 2003, **302**, 1693-1694.
13. G. A. Pino, C. Dedonder-Lardeux, G. Grégoire, C. Jouvet, S. Martrenchard and D. Solgadi, *J. Chem. Phys.*, 1999, **111**, 10747-10749.
14. G. Pino, G. Grégoire, C. Dedonder-Lardeux, C. Jouvet, S. Martrenchard and D. Solgadi, *Phys. Chem. Chem. Phys.*, 2000, **2**, 893-900.
15. A. L. Sobolewski, W. Domcke, C. Dedonder-Lardeux and C. Jouvet, *Phys. Chem. Chem. Phys.*, 2002, **4**, 1093–1100.
16. C. Tanner, C. Manca and S. Leutwyler, *Science*, 2003, **302**, 1736-1739.
17. C. M. Tseng, Y. T. Lee and C. K. Ni, *J Chem Phys*, 2004, **121**, 2459-2461.
18. O. David, C. Dedonder-Lardeux and C. Jouvet, *Int. Rev. Phys. Chem.*, 2002, **21**, 499-523.
19. T. Förster, *Z. Elektrochem.*, 1950, **54**, 531.
20. D. M. Hercules and L. B. Rogers, *Spectrochim. Acta*, 1959, **15**, 393-408.
21. H.-S. Andrei, N. Solca and O. Dopfer, *Phys. Chem. Chem. Phys.*, 2004, **6**, 3801–3810.
22. E. R. Bernstein, *J. Phys. Chem.*, 1992, **96**, 10105-10115.
23. C. M. Harris and B. K. Sellnge, *J. Phys. Chem.*, 1980, **84**, 1366-1371.
24. M. F. Hineman, G. A. Brucker, D. F. Kelley and E. R. Bernstein, *J. Chem. Phys.*, 1992, **97**, 3341-3347.
25. D. F. Kelley and E. R. Bernstein, *Chem. Phys. Lett.*, 1999, **305**, 230–232.
26. S. K. Kim, J.-K. Wang and A. H. Zewail, *Chem. Phys. Lett.*, 1994, **228**, 369-378.
27. R. Knochenmuss, *Chem. Phys. Lett.*, 1998, **293**, 191–196.
28. R. Knochenmuss, *Chem. Phys. Lett.*, 1999, **305** 233–237.
29. C. Lakshminarayan and J. L. Knee, *J. Phys. Chem.*, 1990, **94**, 2637-2643.
30. S. Leutwyler, T. Burgi, M. Schiitz and A. Taylor, *Faraday Discuss.*, 1994, **97**, 285-297.
31. Y. Matsumoto, T. Ebata and N. Mikami, *J. Chem. Phys.*, 1998, **109**, 6303-6311.
32. Y. Matsumoto, T. Ebata and N. Mikami, *J. Mol. Struct.*, 2000, **552**, 257-271.
33. Y. Matsumoto, T. Ebata and N. Mikami, *J. Phys. Chem. A*, 2001, **105**, 5727-5730.
34. M. Saeki, S. Ishiuchi, M. Sakai and M. Fujii, *J. Phys. Chem. A*, 2001, **105**, 10045-10053.
35. M. Saeki, S. Ishiuchi, M. Sakai, K. Hashimoto and M. Fujii, *J. Phys. Chem. A*, 2010, **114**, 11210–11215.
36. M. Schmitt, C. Jacoby, M. Gerhards, C. Unterberg, W. Roth and K. Kleinermanns, *J. Chem. Phys.*, 2000, **113**, 2995-3001.

37. R. J. Stanley and J. A. W. Castleman, *J. Chem. Phys.*, 1991, **94**, 7744-7756.
38. H. B. Steen, M. K. Bowman and L. Kevan, *J. Phys. Chem.*, 1976, **80**, 482-486.
39. M. N. R. Ashfold, B. Cronin, A. L. Devine, R. N. Dixon and M. G. D. Nix, *Science*, 2006, **312**, 1637-1640.
40. G. Grégoire, C. Jouvet, C. Dedonder and A. L. Sobolewski, *Chem. Phys.*, 2006, **324**, 398-404.
41. O. David, C. Dedonder-Lardeux, C. Jouvet and A. L. Sobolewski, *J. Phys. Chem. A*, 2006, **110**, 9383-9387.
42. T. Ebata, N. Mizuochi, T. Watanabe and N. Mikami, *J. Phys. Chem.*, 1996, **100**, 546-550.
43. M. Esboui, C. Jouvet, C. Dedonder and T. Ebata, *J. Phys. Chem. A*, 2010, **114**, 3060–3066.
44. D. C. Lührs, R. Knochenmuss and I. Fischer, *Phys. Chem. Chem. Phys.*, 2000, **2**, 4335-4340.
45. M. Miyazaki, A. Kawanishi, I. Nielsen, I. Alata, S. Ishiuchi, C. Dedonder, C. Jouvet and M. Fujii, *J. Phys. Chem. A*, 2013, **117**, 1522-1530.
46. T. Shimizu, R. Yoshino, S.-i. Ishiuchi, K. Hashimoto, M. Miyazaki and M. Fujii, *Chem. Phys. Lett.*, 2013, **557**, 19-25.
47. O. Cheshnovsky and S. Leutwyler, *J. Chem. Phys.*, 1988, **88**, 4127-4138.
48. R. Knochenmuss, O. Cheshnovsky and S. Leutwyler, *Chem. Phys. Lett.*, 1988, **144**, 317-323.
49. N. Mataga and Y. Kaifu, *Molecular Physics*, 1964, **7**, 137-147.
50. J. R. Platt, *J. Chem. Phys.*, 1949, **17**, 484-495.
51. M. J. Frisch, G. W. Trucks, H. B. Schlegel, G. E. Scuseria, M. A. Robb, J. R. Cheeseman, G. Scalmani, V. Barone, B. Mennucci, G. A. Petersson, H. Nakatsuji, M. Caricato, X. Li, H. P. Hratchian, A. F. Izmaylov, J. Bloino, G. Zheng, J. L. Sonnenberg, M. Hada, M. Ehara, K. Toyota, R. Fukuda, J. Hasegawa, M. Ishida, T. Nakajima, Y. Honda, O. Kitao, H. Nakai, T. Vreven, J. J. A. Montgomery, J. E. Peralta, F. Ogliaro, M. Bearpark, J. J. Heyd, E. Brothers, K. N. Kudin, V. N. Staroverov, T. Keith, R. Kobayashi, J. Normand, K. Raghavachari, A. Rendell, J. C. Burant, S. S. Iyengar, J. Tomasi, M. Cossi, N. Rega, J. M. Millam, M. Klene, J. E. Knox, J. B. Cross, V. Bakken, C. Adamo, J. Jaramillo, R. Gomperts, R. E. Stratmann, O. Yazyev, A. J. Austin, R. Cammi, C. Pomelli, J. W. Ochterski, R. L. Martin, K. Morokuma, V. G. Zakrzewski, G. A. Voth, P. Salvador, J. J. Dannenberg, S. Dapprich, A. D. Daniels, O. Farkas, J. B. Foresman, J. V. Ortiz, J. Cioslowski and D. J. Fox, Gaussian 09, Revision D.01; Gaussian, Inc.: Wallingford CT, 2010.
52. C. Lakshminarayan, J. M. Smith and J. L. Knee, *Chem. Phys. Lett.*, 1991, **182**, 656-662.
53. S. K. Kim, J. J. Breen, D. M. Willberg, L. W. Peng, A. Heikal, J. A. Syage and A. H. Zewail, *J. Phys. Chem.*, 1995, **99**, 7421-7435.
54. R. Knochenmuss and S. Leutwyler, *J. Chem. Phys.*, 1989, **91**, 1268-1278.
55. J. M. López - de - Luzuriaga, E. Manso, M. Monge and D. Sampedro, *Theor. Chem. Acc.*, 2015, **134**, 55-66.
56. T. Shimizu, S. Yoshikawa, K. Hashimoto, M. Miyazaki and M. Fujii, *J. Phys. Chem. B*, 2015, **119**, 2415-2424.